16th Australasian Fluid Mechanics Conference
Crown Plaza, Gold Coast, Australia
2-7 December 2007

Diagnostic Modelling of an Expansion Tube Operating Condition for a Hypersonic Free Shear Layer Experiment

M. McGilvray[1], J.M. Austin[2], M. Sharma[2], P.A. Jacobs[1] and R.G. Morgan[1]

[1]Centre for Hypersonics
University of Queenland, St. Lucia, QLD, 4067, Australia.

[2] Department of Aerospace Engineering
University of Illinois, Urbana-Champaign, IL, 61801, USA.

Abstract

Computational simulations of the AIR-1 test condition in the University of Illinois' Hypervelocity Expansion Tube were conducted to verify facility operation and to obtain free stream properties that are otherwise difficult to measure. Two types of simulation were undertaken. The first was a one-dimensional simulation of the entire facility and the second was a hybrid simulation, combining a one-dimensional simulation of the shock tube section with a two-dimensional simulation of the acceleration tube. The one-dimensional simulation matched the experimental data well, however the two-dimensional simulation did not initially match the experimental measurements of shock speed and test gas pitot pressure. Further investigation showed the shock speed discrepancy was consistent with air contamination into the acceleration tube and subsequent two-dimensional simulations assuming 10% air contamination showed reasonable agreement with experimental data.

Using data taken from the two-dimensional simulation of the expansion tube as a transient inflow condition, modelling was undertaken of a free shear layer experiment being conducted in the facility. Results from equilibrium, finite rate, and perfect gas models were compared. The finite rate simulation provides the best agreement with experimental Schlieren images, with the simulation capturing the major flow structures seen in experiments.

Introduction

Expansion tube facilities produce high enthalpy, high stagnation pressure flows appropriate for simulating hypervelocity flight. As in most ground testing facilities, the free stream properties, including the gas chemical composition in a high temperature flow, need to be accurately characterized. In an expansion tube, unsteady gas dynamic processes are used to accelerate the flow and the transient behaviour may also be important. The high stagnation pressures and short test times result in a challenging environment in which only a few flow properties are able to be measured. Simple perfect gas calculations [16] can provide rough estimates of flow properties. However nonideal processes such as diaphragm rupture, viscous and high-temperature gas effects can alter the flow significantly from these calculations. Therefore computational simulations are needed both to provide verification of facility operation and to obtain a complete description of the free stream properties. Computational simulations have been conducted of a 4 km/s (design Mach number 7.29) air test condition, labelled AIR-1, in use at the Hypervelocity Expansion Tube (HET) facility. A one dimensional simulation of the entire facility and a two dimensional simulation of the acceleration tube were combined.

Current experiments in the HET facility are examining the effects of non-equilibrium chemistry on free shear layers. Asymmetric wedges are used to produce a Mach reflection from which free shear layers are generated at the two shock triple points. To date, there is no analytical means of predicting Mach stem height and growth rate for asymmetric wedges. Also this shock reflection process upstream of the shear layers is highly dependent on the history of the flow. In the case of an expansion tube, the test gas is both transient and preceded by the high temperature, low density acceleration gas. In addition, short time of flight through the experiment and the high-enthalpy conditions suggest finite rate chemical reactions will need to be considered. Therefore, computational simulations that incorporate both the unsteady flow and finite rate chemistry effects are used when calculating the flow field properties. Using the flow data at the exit of the acceleration tube, a two-dimensional simulation has been conducted of the hypersonic free shear layer experiment in the second half of this paper.

HET Facility and Measurement Capabilities

The HET facility is located at the University of Illinois at Urbana-Champaign and was commissioned in 2005. It is a cold driven facility with a bore diameter of 152mm and length of 9.5m. The facility consists of three sections: the driver, driven, and accelerator sections, initially separated by two diaphragms. The driven section is often referred to as the shock tube section. The test gas, initially in the shock tube, is accelerated first by a shock wave and subsequently by an unsteady expansion. A full description of the facility, measurement capabilities and facility operation can be found in Dufrene et al. [3].

The flow condition of interest for this work is the AIR-1 condition which has a design flow speed of 3980m/s at a Mach number of 7.29. The initial conditions for the AIR-1 condition can be seen in Table 1, where it can be noted that the accelerator gas is presumed to be pure helium. Shock tube static pressure and shock speed measurements, test section pitot pressure surveys and shock speed measurements, and schlieren measurements of shock angles over wedge and cone geometries were made to verify facility operation. The test gas Mach number was calculated to be 7.1 from the experimentally measured pitot pressure and shock angles [3], assuming theoretical static pressure and a specific heat ratio of 1.4. The static pressure is yet to be measured in the acceleration tube due to large vibrations in this section and low pressures giving a poor signal to noise ratio.

Table 1: Fill parameters for AIR-1 condition

Tube	Initial pressure	Gas composition
driver	4235.0 kPa	100% helium
shock	1.5 kPa	100% air
acceleration	26.6 Pa	100% helium

Computational Simulations

A two-step approach is taken to modelling the expansion tube to reduce complexity and computational time requirements [8]. First, a one dimensional simulation is conducted of the entire tube using the *L1d* [7] code, which includes frictional losses over diaphragms and viscous effects. Then, to account for boundary layer growth and radial variations, a two-dimensional simulation (using the Navier-Stokes solver *mbcns2* [6]) is conducted of the acceleration tube flow after the secondary diaphragm burst. This axisymmetric simulation uses data calculated directly before the secondary diaphragm from the one-dimensional simulation as a transient inflow condition. This hybrid approach has been shown to give good agreement with experimentally measured conditions, especially at low enthalpy conditions where an equilibrium gas model can be used [8, 11].

One-Dimensional Flow Model

The one dimensional simulation of the facility used the Lagrangian *L1d* code with initial conditions given in Table 1 for the AIR-1 condition. The geometric arrangement of the modelled facility can be seen in Figure 1, where the upstream end of the driver section was set to be a fixed wall and the downstream end of the acceleration tube was set to be free (open). At the start of the simulation, the primary diaphragm was assumed to have burst and the secondary diaphragm was assumed intact. The secondary diaphragm was set to a burst pressure of 25 kPa with a zero hold time. A loss region with a k factor of 0.5 is applied over a distance of 0.25 m both sides of the primary and secondary diaphragms to model the effects of finite opening time and area changes. The viscous terms were included, whereby the boundary-layer effects of wall fraction and heat transfer were applied along the tube. The *L1d* code uses full developed pipe flow correlations to correct locally for the momentum and energy loss from the Lagrangian cells. An equilibrium gas model was used for the test gas and perfect gas for the helium accelerator gas. The simulation used 1050 nodes in total, with clustering of the gas cells within the acceleration tube towards the secondary diaphragm.

Generally, the simulation was found to match the experimentally obtained measurements quite well (shown in Table 2). The numerically calculated primary shock speed matches the experimental shock speed measurement (Figure 2) of 2100±43 m/s. The secondary shock speed in the accelerator section was computed to be 5609 m/s, which is well above the experimental shock speed measurement of 4148 m/s. It can be noticed that the effects of shock attenuation are quite minimal in the simulation. Comparison of the experimentally measured shock tube pressure with the simulation in Figure 3, shows a good agreement in pressure level. Although the simulation sees a disturbance at the same time the static pressure rises in the experimental measurement, the static pressure doesn't rise for another 0.4 ms. Using the perfect gas relationships of Trimpi [16], the static pressure in the acceleration tube is calculated to be 998 Pa, similar to the simulation result.

In the actual facility, the mass loss from the free stream to the boundary layer causes the shock to attenuate and the interface to accelerate, creating a velocity gradient across the shocked gas slug. Mirels theory [12] can be used to estimate the time between the interface and the shock. Using the properties taken from the *L1d* simulation of shock speed and post shock conditions, the estimated time between shock and interface is compared with the ideal gas predictions (i.e. constant wave speed along the tube) in Figure 4 for both the shock and acceleration tubes. The experimentally observed increase in the post-shock pressure (Figure 3a) coincides with the arrival of the driver-test gas interface as predicted by Mirels theory. The increase in

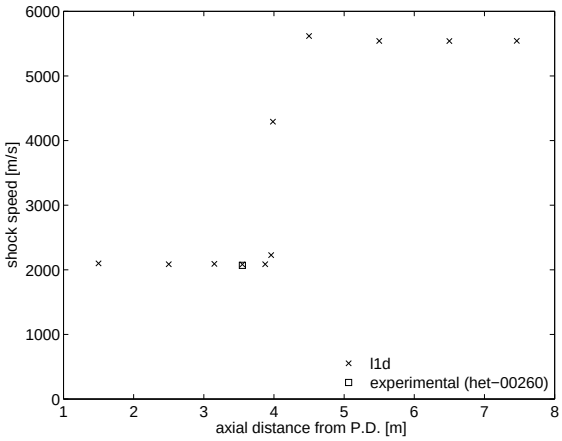

Figure 2: Comparison of *L1d* and experimental shock speeds

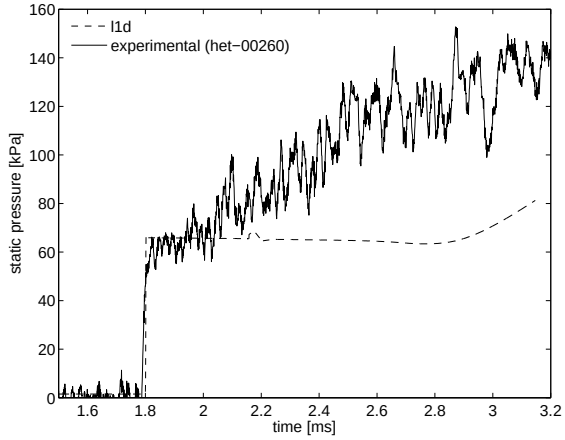

(a) Shock tube - 3.8 m from primary diaphragm

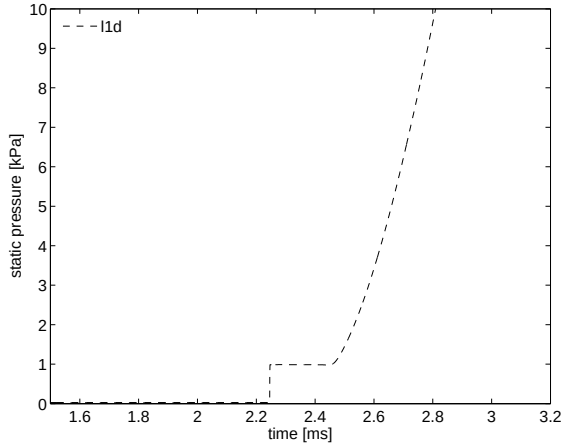

(b) Acceleration tube - 6.0 m from primary diaphragm

Figure 3: Comparison of experimental measurements of static pressure in the shock tube

driver pressure may be caused by the area constriction at the diaphragm cutter located at the primary diaphragm.

The test gas pitot pressure of 66.7 kPa estimated by the *L1d* simulation agrees quite well with the experimentally measured values, Figure 5. The test time is also seen to match with 105 μs of test time before the trailing edge of the unsteady expansion.

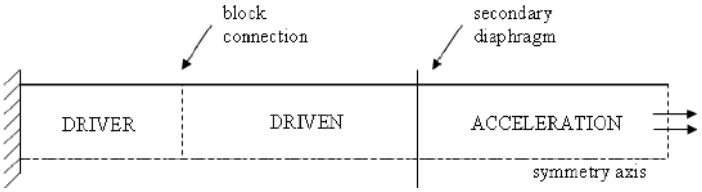

Figure 1: Geometric arrangement for *L1d* simulation

Due to the one dimensional nature of the simulation, the Mirels effect [12] of reduction in acceleration gas slug length due to boundary layer entrapment cannot be seen. The experimentally observed time between the incident shock and the contact surface is seen to match the Mirels predictions shown in Figure 4b quite well. However, at this point, it cannot be explained why the experimentally measured acceleration gas has a pitot pressure approximately twice the predicted value of the simulation.

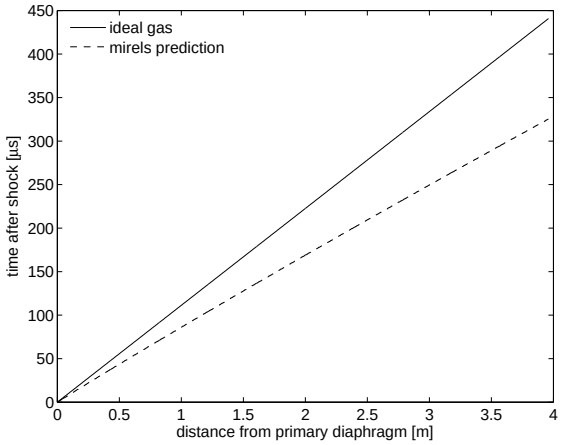

(a) Shock tube

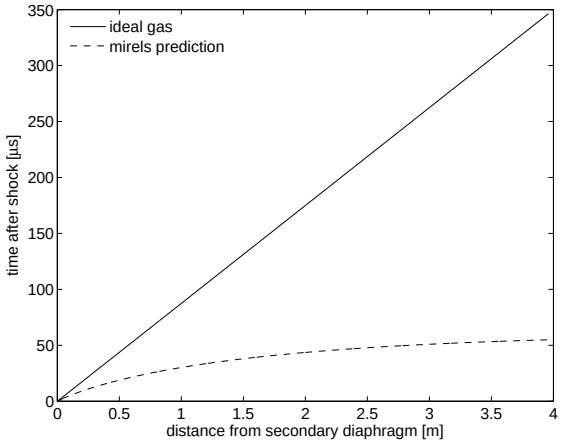

(b) Acceleration tube

Figure 4: Predictions of time between shock and interface using free stream conditions from *L1d* simulation

Two-Dimensional Flow Model

An axisymmetric simulation of just the acceleration tube was conducted using *mbcns2*. This calculation used as an inflow condition, the transient flow data at the downstream-end of the shock tube as estimated by the one-dimensional simulation. An equilibrium gas model for the air test gas and a perfect gas

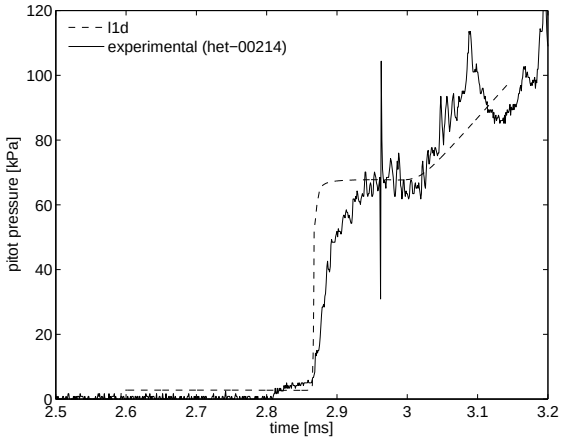

Figure 5: Comparison of *L1d* and experimental pitot pressure in test section, located 54mm downstream of the tube exit. A noise spike occurs due to the Schlieren system flashlamp.

model of the helium acceleration gas was used. Viscous effects were modeled using the Baldwin-Lomax turbulence and transition model along the tube wall. The tube geometry can be seen in Figure 6, with 40 blocks actually used in the simulation. Overall, the simulation had a grid resolution of 4000 cells axially (also another 15 cells for the shock tube) and 80 cells radially, which had been shown to produce reasonable results in another study [8].

The estimated flow properties from the axisymmetric simulation differed significantly from the *L1d* results, and from experimentally measured values, as seen in Table 2. This is due to a large shock attenuation shown in Figure 7 associated Mirels' effect, causing a drop in the post-shock static pressure and temperature. The velocity of the flow, however, is quite high due to the acceleration of the interface which can be predicted in the two-dimensional simulation. Although the Mach number during the test period is increased due to a lower temperature, the Pitot pressure is lower than experimental measurements due to the low static pressure. As discussed above, although the *L1d* Pitot pressure matches the experimental data well for the test gas, the acceleration gas Pitot pressure is low. Similar behaviour of low pitot pressure in the acceleration slug when compared with the experimental measurement was also noted in the two-dimensional simulation even though the static pressure was reduced.

Air Contamination in the Acceleration Tube

The computational simulations were not able to match the measured pitot pressure in the test section satisfactorily although the shock tube conditions match quite well. A possible cause of this discrepancy could be air contamination in the acceleration tube due to residual air from the evacuation procedure and/or air leakage during the experiment. Due to the low molecular weight of helium, only a small amount of air contamination can

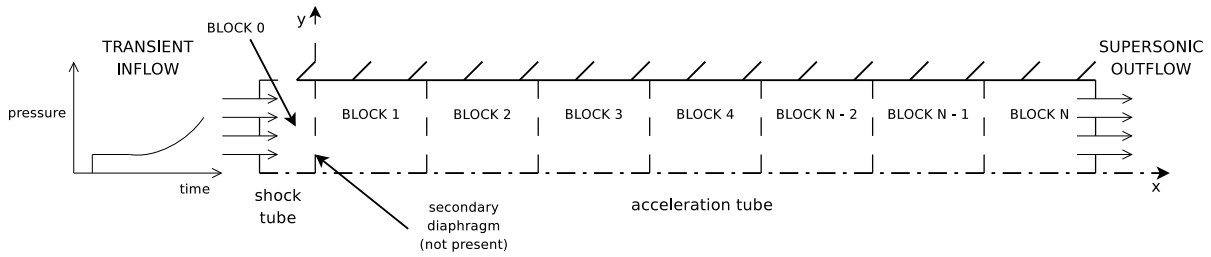

Figure 6: Geometric arrangement for *mbcns2* simulation

Table 2: Comparison of flow conditions from simulations and experiments for Air-1 condition with pure helium acceleration gas. State 7 is the test gas, state 2 is behind the incident shock. U_s is the shock velocity. (Nomenclature as in [11].)

	Experimental	*L1d*	*mbcns2*
U_{s1}, m/s	2069	2100	-
$p_{2,static}$, kPa	65	66	-
U_{s2}, m/s	-	5609	4200
M_7	7.11	7.29	8.02
T_7, K	-	779	680
$p_{7,static}$, Pa	-	998	670
$p_{7,pitot}$, kPa	64	66.7	56
U_7, m/s	4148	4037	4180
ρ_7, g/m^3	-	4.3	3.54
test time, μs	100	105	100

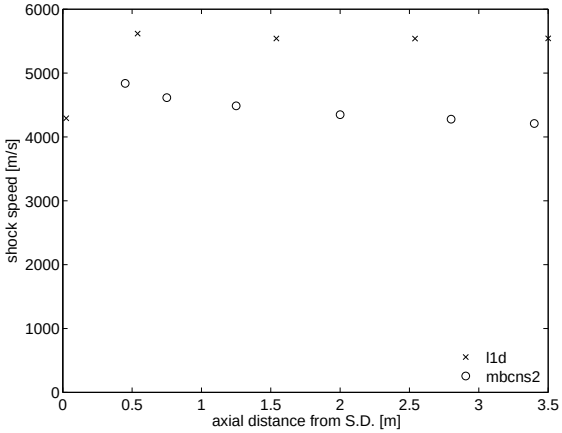

Figure 7: Comparison of shock speed from *L1d* and *mbcns2* simulations

produce a significant change in properties. This can quite easily occur (and is difficult to overcome) especially with the reasonably low initial pressures of approximately 26 Pa (absolute) and low molecular weight gases (helium) used in an acceleration tube which has numerous leak paths (sensor mountings, sliding seals, diaphragm seals). The issue of residual air was attempted to be mitigated by a procedure whereby the acceleration tube was evacuated to a low pressure of 40 Pa, flushed with helium to a large pressure and again evacuated to the final pressure of 26 Pa. Despite such a precaution, however, air contamination due to leakage into the tube still remains a possibility.

Simulations were undertaken using hypothetical contamination levels, in order to estimate the extent of air leakage by comparison to experimental results. As the contamination only occurs in the acceleration tube, the previously described one-dimensional simulation results for the shock tube were again be used as inflow into the axisymmetric calculation. Air contamination levels of 10% and 20% (by volume) were studied using a ideal gas mixture in the acceleration tube and perfect gas properties for the helium component and equilibium properties for the air component. Due to recent code changes in the turbulence model, the simulation was laminar instead of the turbulent simulation performed for the pure helium simulation.

Table 3 and Figure 8 show a comparison of the flow properties in the test period with different levels of air contamination. A number of effects are seen for increasing contamination levels; the shock speed more closely approximates the experimental value and the level of shock attenuation decreases. An increase in the static pressure across the shock in the acceleration section is also seen due to the decrease in the unshocked accleration gas. As Figure 8a and Table 3 illustrate, increasing the air contamination to 10% raises the pitot pressure towards experimentally obtained value of 64 kPa. Assuming 20% contamination, the computational result exceeds the experimentally measured pitot pressure.

Table 3: Comparison of flow conditions of varying levels of air contamination in the accelerator gas from CFD simulations. State 7 is the test gas, state 2 is behind the incident shock. U_s is the shock velocity.

	0% air	10% air	20% air
U_{s2}, m/s	4200	4105	3925
M_7	8.10	7.20	6.55
T_7, K	680	875	870
$p_{7,static}$, Pa	670	1040	1555
$p_{7,pitot}$, kPa	56	69	86
U_7, m/s	4180	3998	3813
ρ_7, g/m^3	-	4.70	6.32
test time, μs	100	100	100

A comparison between the 10% air contamination simulation and experimentally measured Pitot pressure is seen in Figure 9 and shows reasonable agreement, although the experimentally measured Pitot pressure is a little low. This suggests that the likely contamination level is more likely to be approximately

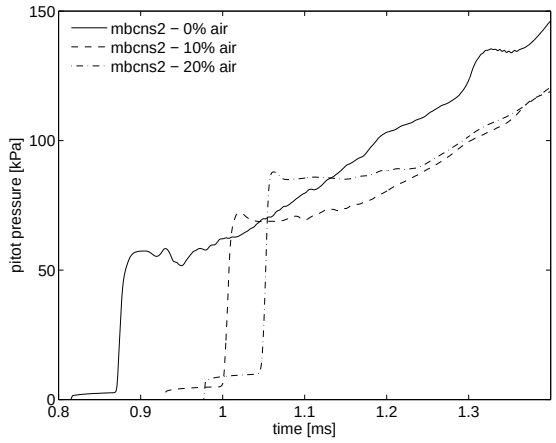

(a) Pitot pressure

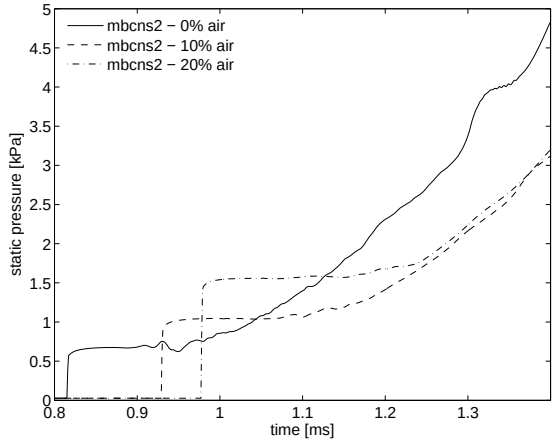

(b) Static pressure

Figure 8: Comparison of flow properties at tube exit of *mbcns2* simulations for varying air contamination levels

8%. The test period between the interface and unsteady expansion is also seen to be in agreement with a test time of 100 μs. The acceleration slug Pitot pressure level is now consistent with experimental measurement, however, the estimated acceleration slug duration is now longer then that measured experimentally. A possible explanation of this behaviour could be due to the finite start up time associated with the Pitot pressure measurements using shrouded transducers, especially at low pressure conditions. This sensor behaviour could also explain the broader accelerator-test gas interface seen experimentally, with the test gas taking approximately 60 μs to reach 64 kPa level of the experimental measurement.

Based on these results, it appears that a value of 10% is an acceptable rough estimate of the acceleration section air contamination level. A comparison between the 10% air contamination simulation and experimentally measured Pitot pressure is seen in Figure 9 and shows reasonable agreement, although the experimentally measured Pitot pressure is a little low. Recent experimental measurements have shown this prediction is reasonable, as the secondary shock speed was measured by staggering Pitot probes in the test section and found to be 4148$\pm$47 m/s. For a 10% contamination level, the acceleration slug pitot pressure level is now consistent with experimental measurement, however, the calculated acceleration slug duration is now longer then that measured experimentally. A possible explanation for the discrepancy is the response time associated with shrouded transducers. This explanation is also consistent with the broader accelerator-test gas interface seen in experiments, with the simulation predicting 20 μs to reach the 64 kPa compared to 60 μs in the experiments.

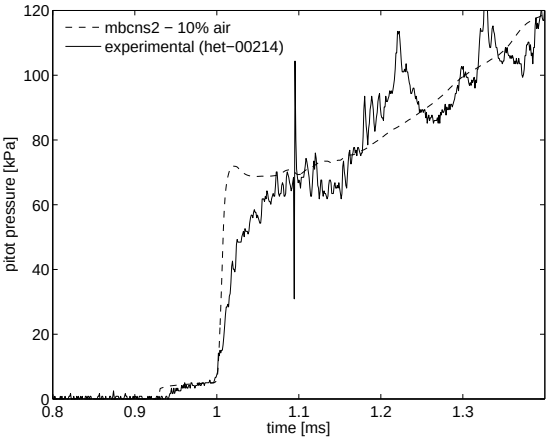

Figure 9: Comparison of Pitot pressure between experiment and CFD for 10% air contamination

Hypersonic Free Shear Layer Simulations

The impact of high temperature, real gas effects such as vibrational excitation and chemical dissociation/recombination on a canonical free shear layer flow is currently being investigated in the HET facility. Such molecular effects can significantly affect hydrodynamic stability and transition in aerodynamic applications. For example, thermochemical effects have been observed to alter both the mean flow profile and stability of boundary layer flows [9, 15, 5].

In the experimental setup, Figure 10, asymmetric opposing wedges are used to produce a Mach reflection with two free shear layers generated at the shock triple points. The shear layers separate two supersonic (relatively cold) gas streams and a subsonic (relatively hot) gas stream, resulting in a high convective Mach number within each shear layer. The experimental configuration was chosen to provide well-characterized shear layer inflow conditions which can be calculated once the free stream conditions and the shock angles are known, and to avoid boundary layer complications associated with splitter-plate experiments. In order to minimize three dimensional effects such as wedge edge reflection [14], the wedges were designed with inlet aspect ratios of 1.25 and wedge aspect ratios of 5.

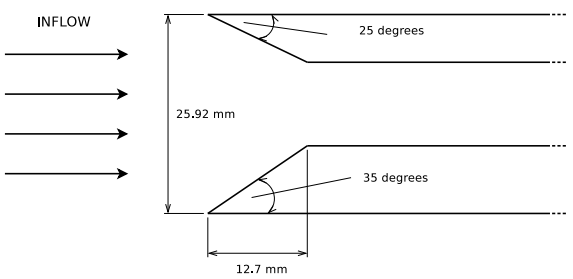

Figure 10: Hypersonic free shear layer experiment schematic

Current experimental work is concentrating on highly resolved Schlieren visualization of the shear layer structure. The computational simulations can provide valuable information about the free stream and shear layer inflow conditions for further analy-

sis with spatial linear stability theory. Another aspect of interest is the shock reflection process between asymmetric wedges where there are significant effects of nonequilibrium chemistry [2]. The high energy and density flow conditions required to create nonequilibrium chemistry effects can be produced by an expansion tube. Also, other effects such as hysteresis starting as a regular to Mach reflection may be able to be tested in an expansion tube [1]. Computational modelling can also be used to examine differences in the flow properties and structures due to the type of thermochemical model (*i.e.* perfect gas *vs* equilibrium chemistry *vs* finite rate chemistry).

Numerical simulations of the free shear layer experiment were conducted using *mbcns2*. The simulation geometry is shown in Figure 11, where the flow domain is broken into 16 blocks with flow entering the simulation from the left and exiting from the right. Each of these blocks has a structured grid, with 100 cells spanning each side of the block with 160000 cells in total. A grid resolution study using both a coarser and finer grids by 50% had negligable effects on the flow. Although the simulations were setup for the inclusion of viscous effects with fixed temperature walls, only inviscid results are presented within this paper. Calculations were run for three different gas models for the test and accelerator section gases (air and helium respectively): a perfect gas mixture, air with equilibrium chemistry using the NASA *CEA* code [10], and finite rate chemistry with helium acting as an inert molecule. The gas was assumed to not be ionised and contained six species; N_2, O_2, NO, N, O and He. The reaction scheme for the finite rate simulation was a reduced form of that given by Gupta [4] as shown in Table 4 with the Arrhenius rates of reaction constants given for the forward and reverse reactions. All third-body efficiencies were 1.0 except for species N in the second equation which was 0.0. Transient properties at the acceleration tube exit at 10 mm above the centreline in the 10% air contamination simulation were used across the entire inflow boundary for the inflow conditions. These properties are shown in Figure 12 for the simulation time of 250 μs, where the composition of the inflow gas for the finite rate simulation is also given. The equilibrium simulation air mass fraction is the summation of all the components excluding helium.

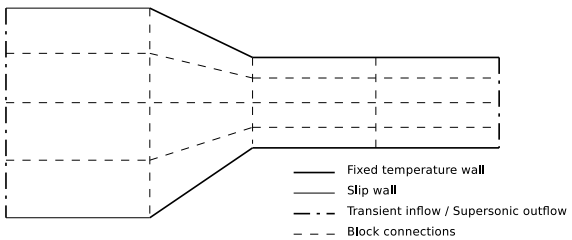

Figure 11: Schematic of numerical simulation setup for free shear layer experiment

Gas Model Comparison

In Figure 13, an experimental Schlieren image with the knife edge orientated in the horizontal plane is compared to computational Schlieren images for the three different gas models described previously. As the wedges are not confined in the viewing plane, flow spillage out the sides of the wedges results in the density gradients picked up by the Schlieren image appearing smeared. The gas chemistry is found to have a strong influence on the flow structure.

The perfect gas simulation does not produce a Mach reflection or supersonic starting of the inlet. Due to the flow restriction in the two dimensional simulation not allowing side spillage as would occur experimentally, the area change is too great in the

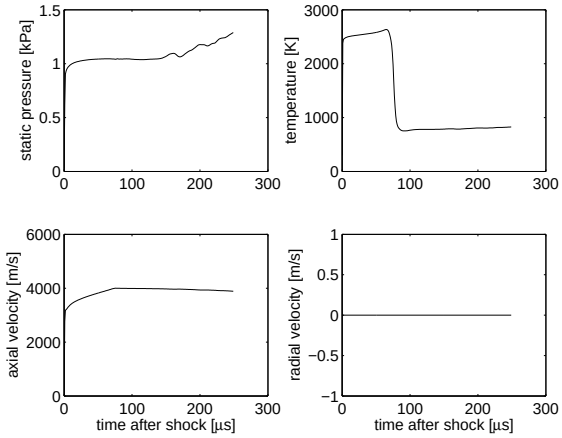

(a) flow properties

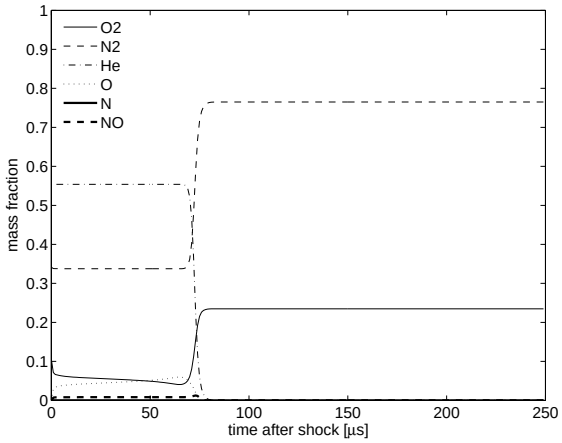

(b) flow composition for finite rate simulation

Figure 12: Transient inflow conditions from axisymmetric simulation of expansion tube

perfect gas simulation and a normal shock is produced before wedge compressions.

In contrast, the equilibrium simulation results in a Mach stem that is further downstream than observed in the experiments. It is suggested that the higher density in the converging subsonic stream behind the Mach stem predicted by the equilibruim calculation (due to the lower temperature) allows a smaller inlet area through which to achieve the mass balance [13]. The physical manifestation of such an argument is that the Mach stem height reduces as it moves downstream. Separated regions of flow in the enclosed area between the wedges are also seen in both the equilibrium and finite rate simulations.

The finite rate chemistry simulation comes the closest to simulating the flow behaviour seen experimentally, with the a similar Mach stem produced and similar shear layer interactions and downstream shock structure. The Mach stem appears somewhat further downstream than in experiments. Slightly lower air contamination levels or wedge mis-alignment issues could account for this difference, however, further work is required for a more definitive answer.

To investigate the differences between the experiment and computational simulations, an overlay of colour density contours from the transient finite-rate simulation is overlaid on top of the experimental Schlieren image in Figure 14. Note that the two wedges in the experiment are slightly misaligned and the

Table 4: Reaction scheme and Arrhenius coefficients for finite rate simulation

reaction	k_f			k_b		
	A	n	E_a	A	n	E_a
$O_2 + M \Longleftrightarrow 2O + M$	3.61e18	-1.0	5.94e4	3.01e15	-0.5	0.0
$N_2 + M \Longleftrightarrow 2N + M$	1.92e17	-0.5	1.131e5	1.09e16	-0.5	0.0
$N_2 + N \Longleftrightarrow 2N + N$	4.15e22	-1.5	1.131e5	2.32e21	-1.5	0.0
$NO + M \Longleftrightarrow N + O + M$	3.97e20	-1.5	7.56e4	1.01e20	-1.5	0.0
$NO + O \Longleftrightarrow O_2 + N$	3.18e9	1.0	1.97e4	9.63e11	0.5	3.6e3
$N_2 + O \Longleftrightarrow NO + N$	6.75e13	0.0	3.75e4	1.5e13	0.0	0.0

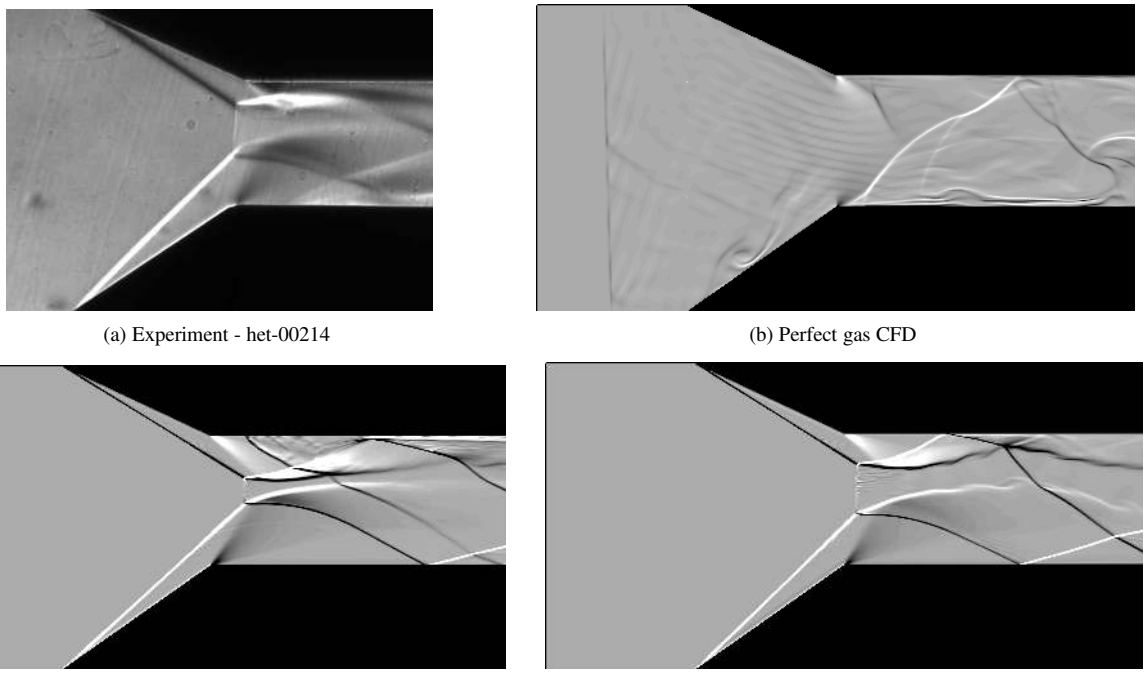

(a) Experiment - het-00214

(b) Perfect gas CFD

(c) Equilibrium CFD

(d) Finite rate CFD

Figure 13: Schlieren images of free shear layer experiment at $150\,\mu s$ after the shock

wedge spacing is slightly smaller than in the simulations. These geometric changes may contribute to the difference in Mach stem location discussed above. Despite these differences, good agreement is seen between simulation and experiments.

The test flow produced by the expansion tube although initially experiences non-equilibrium chemistry effects when shocked and rapidly expanded, the long duration period of travelling down the acceleration tube allows the gas to reach chemical equilibrium. However due to the small length scales of the experiment, the gas may not be capable of reaching chemical equilibrium. To investigate whether the flow in the finite-rate chemistry simulation reaches equilibrium, static temperature is extracted from streamlines passing through the high temperature subsonic region and the low temperature supersonic region behind the incident and reflected shock for the top wedge (Figure 15). It should be noted that, due to the Mach stem being further downstream in the equilibrium calculation, the initial rise in temperature occurs at a location further downstream than for the finite-rate chemistry case. Because the flow is being accelerated through the converging slip stream, the temperature does not relax to a particular equilibrium level. However, using the NASA *CEA* code, the predicted levels of equilibrium gas composition can be calculated for the given static temperature and pressure along a streamline. This has been undertaken for three locations along a subsonic streamline for the finite-rate simulation as shown in Figure 15. Comparison of the equilibrium and the simulated gas compositions (Table 5) reveals that the gas composition is not close to reaching equilibrium. The finite-rate simulation also shows the estimated levels of NO are reasonably high, while the production of N is minimal.

Flow establishment

To examine the overall effect of the time-dependant flow through the experiment, Figure 16 shows temperature contours from the finite rate simulation for various times during the test time. A Mach stem is produced in the middle of the flow, with subsonic flow behind it. The flow that has passed through the oblique shocks remains supersonic and passes through an expansion fan generated at the wedge corner. The supersonic and subsonic flows interact in a shear layer region. As the flow

Table 5: Gas composition behind Mach stem from simulation (f.r.) and using *CEA* to calculate equilibrium values (eq.)

x	p	T	m_{f,O_2}		m_{f,N_2}		$m_{f,NO}$		$m_{f,O}$		$m_{f,N}$	
$[mm]$	$[kPa]$	$[K]$	f.r.	eq.	f.r.	eq.	f.r.	eq.	f.r.	eq.	f.r.	eq.
15	62.933	6196	0.1827	0.0002	0.7498	0.5802	0.0316	0.0072	0.0354	0.2309	0.0006	0.1816
20	38.304	5196	0.1308	0.0007	0.7225	0.7205	0.0898	0.0124	0.0562	0.2275	0.0007	0.0388
25	16.356	4280	0.1277	0.0039	0.7212	0.7501	0.0934	0.0188	0.0574	0.2209	0.0003	0.0053

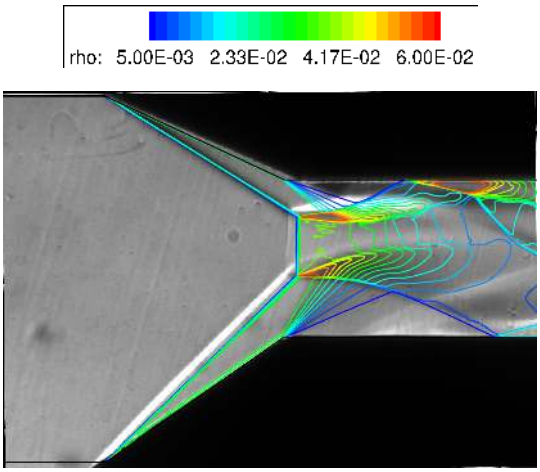

Figure 14: Experimental Schlieren image (het-00214) of free shear layer experiment at 150 μs after the passage of the shock. This image is overlaid with density contours from transient finite rate simulation at 150 μs. (Density in kg/m^3.)

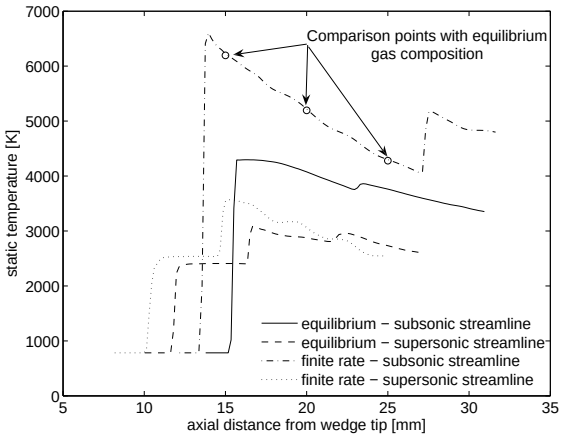

Figure 15: Temperature along streamlines in both the subsonic and supersonic regions of the flow

structure establishes after the passing of the acceleration gas, the Mach stem is seen to move slightly downstream. The flow is fully established about 140 μs after initial shock passage, about 70 μs into the test time.

Conclusions

A combined one-dimensional and two-dimensional numerical simulation procedure has been used to model the newly commissioned Hypervelocity Expansion Tube. Anomalies in the data provided by the two-dimensional simulation, point to the possibility of air contamination in the acceleration tube, which can significantly alter flow conditions. These simulations also provide estimates for the transient free stream conditions for flow over experimental models. The simulation of a free shear layer experiment currently being conducted in the expansion tube was carried out. Here, high temperature effects on shear layers stability and structure was explored and good agreement was seen between computational and experimental Schlieren images. Perfect gas, equilibrium, finite-rate thermochemical models were examined, with finite-rate simulations providing the best match to the experimentally observed Mach reflection structure. The simulations have provided useful information about test gas inflow conditions and shear layer properties to be used in further modelling efforts.

Acknowledgements

The authors would like to acknowledge the University of Queensland's graduate research office for financial support in the form of a Graduate Research Student Travel Award for Matthew McGilvray to visit the University of Illinois. All the simulations detailed in this paper were undertaken on the Blackhole cluster computer located at the Centre for Hypersonics, University of Queensland. Financial support for the cluster computer was provided by SUN Microsystems and by the Queensland State government under the Smart State program. We thank Rowan Gollan, Carolyn Jacobs, Daniel Potter and Marlies Hankel for running the University of Queensland cluster computer. Also, help with the finite rate simulations was provided by Daniel Potter and Rowan Gollan.

References

[1] Ben-Dor, G., Ivanov, M., Vaislev, E.I. and Elperin, T., "Hysteresis processes in the regular reflection ↔ Mach reflection transition in steady flows," *Progress in Aerospace Sciences*, Vol. 38, 2002, pp. 347-387.

[2] Burtschell, Y., Zeitoun, D.E. and Ben-Dor, G., "Steady shock wave reflections in thermochemical nonequilibrium flows," *Shock Waves*, Vol 11, 2001, pp. 15-21.

[3] Dufrene, A. and Sharma, M. and Austin, J.M., "Design and Characterization of a Hypervelocity Expansion Tube Facility," 45th AIAA Aerospace Sciences Meeting, Reno, Nevada, AIAA Paper 2007-1327, January, 2007, also accepted to J. Prop. Power.

[4] Gupta, R.N., Yos, J.M., Thompson, R.A. and Lee, K.-P., "A Review of Reaction Rates and Thermodynamic and Transport Properties for an 11-Species Air Model for Chemical and Thermal Nonequilibrium Calculations to 30 000 K," NASA Reference Publication 1232, 1990.

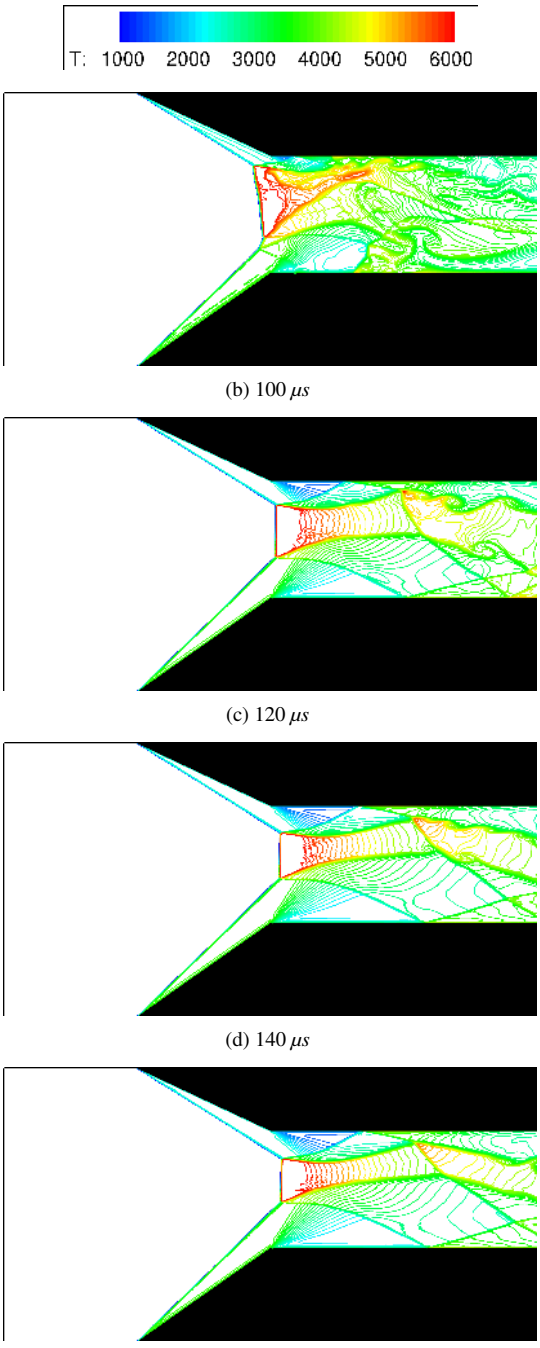

(b) 100 μs

(c) 120 μs

(d) 140 μs

(e) 160 μs

Figure 16: Temperature contours of transient inflow finite rate chemistry simulation of free shear layer experiment. (Temperature in degrees K.)

[5] Hudson M.L., N. Chokani and G.V. Candler, "Linear stability of hypersonic flow in thermochemical nonequilibrium" *AIAA Journal*, Vol. 35, No. 6, 1997, pp. 958-964.

[6] Jacobs, P. A., "MB_CNS: A computer program for the simulation of transient compressible flow," Report 10/96, Department of Mechanical Engineering, University of Queensland Brisbane Qld 4072.

[7] Jacobs, P. A., "Shock tube modelling with L1d," Report 13/98, Department of Mechanical Engineering, University of Queensland Brisbane Qld 4072.

[8] Jacobs, P. A., Silvester, T. B., Morgan, R. G., Scott, M. P., Gollan, R. J. and McIntyre, T. J., "Super-orbital expansion tube operation: Estimates of flow conditions via numerical simulation," 43rd AIAA Aerospace Sciences Meeting, Reno, AIAA Paper 2005-694, January 2005.

[9] Malik M.R. and E.C. Anderson, "Real gas effects on hypersonic boundary-layer stability" *The Physics of Fluids*, Vol. 3, No. 5, 1991, pp. 803-821.

[10] McBride, B. J. and Gordon, S., "Computer Program for Calculation of Complex Chemical Equilibrium Compositions and Applications II. Users Manual and Program Description." NASA Reference Publication 1311, 1996.

[11] McGilvray, M., Morgan, R. G., Jacobs, P. A. and Ramanah, D., "Boundary Layer Transition in an Expansion Tube at a Low Enthalpy Operating Condition," 45th AIAA Aerospace Sciences Meeting, Reno, AIAA Paper 2007-1328, January 2007.

[12] Mirels, H., "Test Time in Low-Pressure Shock Tubes," *The Physics of Fluids*, Vol. 6, No. 9, 1963, pp. 1201-1214.

[13] Mouton, C.A. and Hornung, H.G., "Mach Stem Height and Growth Rate Predictions," *AIAA Journal*, Vol. 45, No. 8, 2007, pp. 1977-1987.

[14] Skews, B.W., "Aspect ratio effects in wind tunnel studies of shock wave reflection transition," *Shock Waves*, Vol. 7, 1997, pp. 373-383.

[15] Stuckert G. and H.L. Reed, "Linear disturbances in hypersonic, chemically reacting shock layers", *AIAA Journal*, Vol. 32, No. 7, 1994, pp. 1384-1393.

[16] Trimpi, R. L., "A Preliminary Theoretical Study of the Expansion Tube, a New Device for Producing High-Enthalpy Short Duration Hypersonic Gas Flows," NACA TR R-133, 1962.